Heat pulse scattering at rough surfaces: reflection

1996 J. Phys.: Condens. Matter 8 1

(http://iopscience.iop.org/0953-8984/8/1/003)

J. Phys.: Condens. Matter **8** (1996) 1–14. Printed in the UK

Heat pulse scattering at rough surfaces: reflection

A G Kozorezov†, T Miyasato‡ and J K Wigmore†

† School of Physics and Chemistry, Lancaster University, Lancaster LA1 4YB, UK
‡ Centre for Microelectronic Systems, Kyushu Institute of Technology, Iizuka, Fukuoka, Japan

Received 28 September 1995, in final form 27 October 1995

Abstract. We have modelled the scattering of heat pulses from rough surfaces, as observed in reflection experiments. The effect of long-range irregularities was calculated in the eikonal approximation. For diffusive scattering from short-range irregularity, an analytic expression was obtained which is valid in the most common experimental arrangements. The model was used to interpret data obtained in heat pulse experiments on buried interfaces in silicon.

1. Introduction

Investigating the scattering of heat pulses on a nanosecond time-scale is a valuable means of studying crystal surfaces and characterizing interface quality of semiconductor microstructures [1]. Many experiments have been carried out, particularly on single crystals of sapphire and silicon, but the interpretations have been almost totally qualitative [2–6]. Both reflection and transmission geometries have been used; in the present paper we limit discussion to reflection only. The technique is very sensitive because the high-frequency phonons typically have wavelengths comparable to the scale of surface irregularity. However, the general theory of such scattering over the full frequency range of phonons comprising a typical heat pulse is extremely complex. Nakayama [7, 8] worked out the scattering cross-section in the limit where the phonon wavelength is much greater than the surface roughness scale. He showed that the process is essentially one of Rayleigh-type scattering following an ω^4-dependence. In the present work we describe calculations carried out for phonons for which the above condition is not satisfied. We model the scattering for phonons with wavelengths comparable to the scale of surface irregularity as an extension of diffusive scattering theory, obtaining an analytic expression which is valid in the most common situations. For phonons with wavelengths shorter than the roughness scale an eikonal approximation is used, in which specular reflection from local mirror spots is shown to be important. Finally we compare our calculations with previously published results of experiments carried out on implanted silicon wafers, in which the scale of surface irregularity could be changed by annealing the sample [9]. A preliminary account of this work was published earlier [10]. We give considerable detail of the individual steps in the theory since we believe that the approach and the results shown have wide applicability.

2. Formulation of the incident flux problem

The rough surface to be considered is shown schematically in figures 1 and 2. The plane of the surface is x–y and the height in the z-direction from the mean plane is described

0953-8984/96/010001+14$19.50

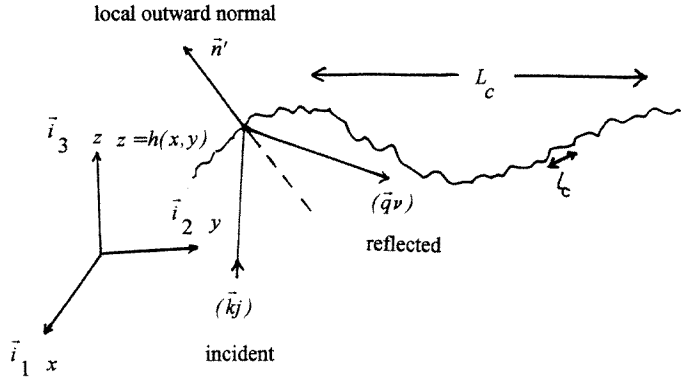

Figure 1. A section of the irregular surface ($\bar{\lambda} \ll L_c$). $\boldsymbol{n}'$ is the local normal vector, $\boldsymbol{k}j$ and $\boldsymbol{q}\nu$ show incident and scattered (reflected) phonons.

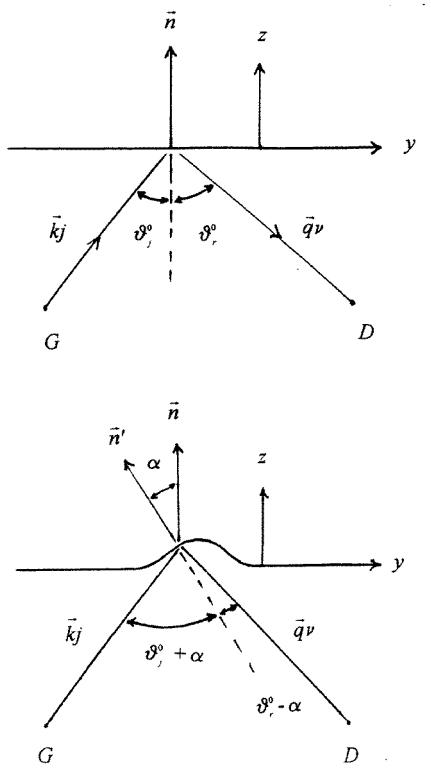

Figure 2. Reflections from ideal (upper figure) and smooth irregular (lower figure) surfaces. α gives the deviation of the local normal vector $\boldsymbol{n}'$ with respect to $\boldsymbol{i}_3$.

by $z = h(x, y)$. Throughout, the incident phonon is described by the suffices $\boldsymbol{k}$, j and the scattered phonon by $\boldsymbol{q}$, ν. We assume $\langle h(x, y)\rangle = 0$, where the brackets stand for the result of statistical averaging over all surface irregularities. We characterize the surface via macroscopic and microscopic scales L_c and l_c respectively assuming $l_c \ll L_c$. We consider

the case where the typical phonon wavelength falls in between l_c and L_c, i.e. $l_c \leq \bar{\lambda} \ll L_c$. Thus, if $L_c \to \infty$ and $\bar{\lambda} \gg l_c$ we arrive at the model used in [7, 8], while in the limit $l_c \to 0$ but keeping L_c finite we come to another extreme case of eikonal approximation.

We start from the eikonal approximation and incorporate the effects due to finite l_c later. Let the source of nonequilibrium phonons be

$$n_{\boldsymbol{k}j}(\boldsymbol{x}, t) = n^0_{\boldsymbol{k}j}\tau_G\,\delta(\boldsymbol{x} - \boldsymbol{x}_G)\,\delta(t). \tag{1}$$

Here $n^0_{\boldsymbol{k}j}$ is a Planck distribution with generator temperature T_G, $\boldsymbol{x}_G$ is the generator coordinate and τ_G is the phonon pulse duration.

For simplicity we assume the crystal to be elastically isotropic and disregard phonon scattering in the bulk. Let the generator and the detector lie in the (yz)-plane:

$$\boldsymbol{x}_G = \begin{pmatrix} 0 \\ -y_0 \\ -z_0 \end{pmatrix} \qquad \boldsymbol{x}_D = \begin{pmatrix} 0 \\ y_0 \\ -z_0 \end{pmatrix}.$$

The energy flux associated with the incident ballistic phonons is

$$\begin{aligned}\boldsymbol{S}(\boldsymbol{x}, t) &= \sum_{\boldsymbol{k}j} \boldsymbol{S}_{\boldsymbol{k}j}(\boldsymbol{x}, t) = \sum_{\boldsymbol{k}j} n^0_{\boldsymbol{k}j}(T_G)\bar{h}\omega_{\boldsymbol{k}j}\boldsymbol{c}_j\,\delta(\boldsymbol{R} - \boldsymbol{c}_j t) \\ &= \bar{h}\left(\frac{\pi}{120}\right)\frac{\boldsymbol{R}}{R^3}\left(\frac{k_B T_G}{\bar{h}}\right)^4 \sum_j \frac{1}{c_j^2}\,\delta(R - c_j t)\end{aligned} \tag{2}$$

where $\boldsymbol{R} = \boldsymbol{x} - \boldsymbol{x}_G$, $\boldsymbol{c}_j$ is the velocity for the $(\boldsymbol{k}, j)$-mode, and $\bar{h}\omega(\boldsymbol{k}, j)$ is its energy. The last step in (2) is the result of straightforward summation over wave vectors $\boldsymbol{k}$. Let $\boldsymbol{x}'$ be the scattering point at the surface and $r_{j\to\nu}(\vartheta)$ be the coefficient of reflection from mode j to mode ν for a given value of incidence angle ϑ. Then, according to reflection laws we may write for the flux incident at $\boldsymbol{x}'$ at the angle Θ

$$\left(\boldsymbol{S}_\nu(\boldsymbol{x}', t)\cdot\frac{\boldsymbol{n}'}{n'}\right) = -\frac{\boldsymbol{R}'\cdot\boldsymbol{n}'}{R'n'}\frac{\bar{h}}{4\pi R'^2}\frac{\pi^2}{30}\left(\frac{k_B T_G}{\bar{h}}\right)^4 \sum_j \frac{r_{j\to\nu}(\vartheta)}{c_j^2}\,\delta(R' - c_j t). \tag{3}$$

3. Scattered flux: general considerations

The kinetic equation for ballistic phonons $(\boldsymbol{q}\nu)$ moving away from the surface after reflection is

$$\frac{\partial N_{\boldsymbol{q}\nu}}{\partial t} + \boldsymbol{c}_\nu\frac{\partial N_{\boldsymbol{q}\nu}}{\partial \boldsymbol{x}} = 0. \tag{4}$$

Rewriting (4) in integral form we can relate the phonon distribution in the bulk at the arbitrary point $\boldsymbol{x}$ and instant of time t to the phonon flux at the surface in the preceding instants of time:

$$\begin{aligned}N_{\boldsymbol{q}\nu}(\boldsymbol{x}, t) = &-\int_{-\infty}^{t} \mathrm{d}t' \int \mathrm{d}\boldsymbol{x}'\;\delta[\boldsymbol{x} - \boldsymbol{x}' - \boldsymbol{c}_\nu(t - t')]\,\delta[z' - h(x', y')] \\ &\times \sum_{\boldsymbol{k}j} r(\boldsymbol{k}j \to \boldsymbol{q}\nu) n^0_{\boldsymbol{k}j}(T_G) c_j \frac{\boldsymbol{R}'\cdot\boldsymbol{n}'}{R'}\,\delta(\boldsymbol{R}' - \boldsymbol{c}_j t').\end{aligned} \tag{5}$$

In (5) we introduced the new entity $r(\boldsymbol{k}j \to \boldsymbol{q}\nu)$ to describe transformation of the incident phonon $\boldsymbol{k}j$ into mode $\boldsymbol{q}\nu$ as a result of either reflection or scattering from the surface. At this stage we incorporate the effect of diffuse scattering ($l_c \ll \bar{\lambda}$) and define $w(\boldsymbol{k}j \to \boldsymbol{q}\nu)$ according to $(\boldsymbol{n}\cdot\boldsymbol{S}_{\boldsymbol{q}\nu}) = -w(\boldsymbol{k}j \to \boldsymbol{q}\nu)(\boldsymbol{n}\cdot\boldsymbol{S}_{\boldsymbol{k}j})$. Thus $w(\boldsymbol{k}j \to \boldsymbol{q}\nu)$ stands for the

probability of elastic conversion at the surface from the $\boldsymbol{k}j$- into the $\boldsymbol{q}\nu$-mode, and $\boldsymbol{S}_{\boldsymbol{q}\nu}$ and $\boldsymbol{S}_{\boldsymbol{k}j}$ are corresponding phonon fluxes. Now the expression for the outward-going phonon flux becomes

$$(\boldsymbol{n}(\boldsymbol{x})\cdot\boldsymbol{c}_\nu)N_{\boldsymbol{q}\nu}(\boldsymbol{x},t) = -[r_{j\to\nu}(\vartheta)(1-w(\boldsymbol{k},j)) + w(\boldsymbol{k}j\to\boldsymbol{q}\nu)]\frac{\boldsymbol{S}_{\boldsymbol{k}j}\cdot\boldsymbol{n}}{\hbar\omega_{\boldsymbol{k}j}}. \tag{6}$$

If we define

$$r(\boldsymbol{k}j\to\boldsymbol{q}\nu) \equiv r_{j\to\nu}(\vartheta)[1-w(\boldsymbol{k},j)] + w(\boldsymbol{k}j\to\boldsymbol{q}\nu)$$

where

$$w(\boldsymbol{k},j) \equiv \sum_{\boldsymbol{q}'\nu'} w(\boldsymbol{k}j\to\boldsymbol{q}'\nu')$$

is the total probability for a phonon of the $\boldsymbol{k}j$-mode to be diffusively scattered into all possible phonon modes, then we again arrive at (5) with the effects of diffuse scattering by short-scale irregularities properly accounted for. Note that

$$\sum_{\boldsymbol{q}'\nu'} r(\boldsymbol{k}j\to\boldsymbol{q}'\nu') = 1$$

as it should for a surface–vacuum interface.

We introduce $I^{spec}(t)$ and $I^{diff}(t)$ in order to describe the different components of the total flux:

$$\begin{aligned} I^{spec}(t) = -\hbar\sum_{\boldsymbol{q}j\nu}\Bigg\langle & c_\nu^2(\boldsymbol{q}\cdot\boldsymbol{i}_3)\int_{-\infty}^{t}\mathrm{d}t'\int\mathrm{d}\boldsymbol{x}'\;\delta[\boldsymbol{x}_D-\boldsymbol{x}'-\boldsymbol{c}_\nu(t-t')]\,\delta[z'-h(x',y')] \\ & \times n^0_{\boldsymbol{q}\nu}(T_G)c_j\frac{((\boldsymbol{x}'-\boldsymbol{x}_G)\cdot\boldsymbol{n}')}{|\boldsymbol{x}'-\boldsymbol{x}_G|}\,\delta\!\left(\boldsymbol{x}'-\boldsymbol{x}_G-c_j\frac{\boldsymbol{q}-\alpha q\boldsymbol{n}'}{|\boldsymbol{q}-\alpha q\boldsymbol{n}'|}t'\right) \\ & \times r_{j\to\nu}(\vartheta)[1-w(\boldsymbol{q}-\alpha q\boldsymbol{n}',j)]\Bigg\rangle \end{aligned} \tag{7}$$

$$\begin{aligned} I^{diff}(t) = -\hbar\sum_{\boldsymbol{k}j,\boldsymbol{q}\nu}\Bigg\langle & w(\boldsymbol{k}j\to\boldsymbol{q}\nu)c_\nu^2(\boldsymbol{q}\cdot\boldsymbol{i}_3)\int_{-\infty}^{t}\mathrm{d}t'\int\mathrm{d}\boldsymbol{x}'\;\delta[\boldsymbol{x}_D-\boldsymbol{x}'-\boldsymbol{c}_\nu(t-t')] \\ & \times\delta[z'-h(x',y')]\,n^0_{kj}(T_G)c_j\frac{\boldsymbol{R}'\cdot\boldsymbol{n}'}{R'}\,\delta(\boldsymbol{R}'-\boldsymbol{c}_jt')\Bigg\rangle. \end{aligned} \tag{8}$$

We discuss first the specular part of the reflected signal. For a fixed $\boldsymbol{q}\nu$-mode only those $\boldsymbol{k}j$ which are related to $\boldsymbol{q}\nu$ by local reflection laws at each point $\boldsymbol{x}$ contribute to the flux $(\boldsymbol{n}\cdot\boldsymbol{c}_\nu)N_{\boldsymbol{q}\nu}(\boldsymbol{x},t)$. We thus demand: (1) that all three vectors $\boldsymbol{k},\boldsymbol{q},\boldsymbol{n}$ lie in the same plane; (2) tangential components of wave vectors for incident and reflected waves are equal if evaluated with respect to local mirror plane; and (3) no frequency change occurs. The conditions (1)–(3) mean that $\boldsymbol{k}=\boldsymbol{q}-\alpha q\boldsymbol{n}$ with

$$\alpha = \frac{\boldsymbol{q}\cdot\boldsymbol{n}}{qn^2} - \frac{1}{n}\sqrt{\left(\frac{\boldsymbol{q}\cdot\boldsymbol{n}}{qn}\right)^2+\left(\frac{c_\nu}{c_j}\right)^2-1}$$

and $\boldsymbol{q}\cdot\boldsymbol{n}<0$.

4. The eikonal approximation: the specular signal

The statistical averaging over the microscopic irregularities with the scale l_c is assumed to have been already performed. Thus, $w(\boldsymbol{k}j \to \boldsymbol{q}\nu)$ coincides with corresponding formulas from [7, 8]. Now we average the result over the macroscopic irregularities. We perform a statistical averaging of (7) while keeping only the zeroth-order approximation for $I^{diff}(t)$, that is, in the limit $L_c \to \infty$. Integration of (7) over $\mathrm{d}\boldsymbol{x}'$ with a Taylor series expansion of the δ-function argument yields

$$I^{spec}(t) = -\overline{h}\int \mathrm{d}\boldsymbol{m}\sum_{\boldsymbol{q}j\nu}\Theta(-q_z)c_\nu n^0_{\boldsymbol{q}\nu}(T_G)qr_{j\to\nu}[1-w(\omega_{\boldsymbol{q}\nu})]\frac{z_0+2y_0m_yq_z/\boldsymbol{q}\cdot\boldsymbol{m}}{t+(1/c_\nu)(q/q_z)z_0}$$
$$\times\delta\left[2y_0\boldsymbol{i}_2+\frac{\boldsymbol{q}}{q_z}z_0-\frac{c_j^2}{c_\nu}\frac{\boldsymbol{q}-\alpha(\boldsymbol{m})q\boldsymbol{m}}{q}\left(t+\frac{1}{c_\nu}\frac{q}{q_z}z_0\right)\right]\langle\delta(\boldsymbol{m}-\boldsymbol{n})\rangle \qquad (9)$$

where in order to perform the statistical averaging we introduced the identity

$$\int \mathrm{d}\boldsymbol{m}\ \delta(\boldsymbol{m}-\boldsymbol{n}) = 1.$$

We also neglected small terms of the order of $\max|h| \ll z_0$, thus disregarding pulse broadening due to small extra paths $\approx\max|h|$ with respect to the much stronger effect of varying local normals and change in the incidence angles. Finally we took the total probability for diffuse scattering at an arbitrary element of the surface as being dependent on phonon energy only, ignoring any possible angular dependence. If we let $\psi(r) = \langle h(r)h(0)\rangle$ be the pair correlation function for smooth surface irregularities, then

$$\langle\delta(\boldsymbol{m}-\boldsymbol{n})\rangle = \frac{1}{(2\pi)^3}\int \mathrm{d}\boldsymbol{Q}\ \exp[\mathrm{i}\boldsymbol{Q}\cdot\boldsymbol{m}]\langle\exp[\mathrm{i}\boldsymbol{Q}\cdot\boldsymbol{n}]\rangle = \frac{\delta(m_z-1)}{2\pi\chi(0)}\exp\left[-\frac{m_x^2+m_y^2}{2\chi(0)}\right]$$

where

$$\chi(0) = -\frac{1}{2}\left.\frac{\partial^2\psi(r)}{\partial r_i^2}\right|_{r=0}.$$

The evaluation of $\langle\exp[\mathrm{i}\boldsymbol{Q}\cdot\boldsymbol{n}]\rangle$ and subsequent integration over $\mathrm{d}\boldsymbol{Q}$ is straightforward.

Substitution of this result into (9) with slight rearrangement of the δ-function term yields

$$I^{spec}(t) = -\frac{\overline{h}}{(2\pi)^4}\frac{1}{z_0}\frac{1}{\chi(0)}\int \mathrm{d}\boldsymbol{m}\ \delta(m_z-1)\exp\left[-\frac{m_x^2+m_y^2}{2\chi(0)}\right]$$
$$\times\sum_{\boldsymbol{q}j\nu}\Theta(-q_z)q\frac{c_\nu^2}{c_j^2}n^0_{\boldsymbol{q}\nu}(T_G)r_{j\to\nu}[1-w(\omega_{\boldsymbol{q}\nu})]\frac{1}{|\alpha(\boldsymbol{m})|}$$
$$\times\frac{z_0+2y_0m_yq_z/\boldsymbol{q}\cdot\boldsymbol{m}}{t+(1/c_\nu)(q/q_z)z_0}\,\delta\left(m_x-\frac{q_x}{q_z}\right)\delta\left[2y_0-z_0\frac{\alpha(\boldsymbol{m})q}{q_z-\alpha(\boldsymbol{m})q}\left(m_y-\frac{q_y}{q_z}\right)\right]$$
$$\times\delta\left[t+\frac{1}{c_\nu}\frac{q}{q_z}z_0-z_0\frac{c_\nu}{c_j^2}\frac{q}{q_z-\alpha(\boldsymbol{m})q}\right]. \qquad (10)$$

This is a general result. It does not depend on particular assumptions about surface roughness other than $\max|h| \ll z_0$. It is obvious that the order of magnitude of $\chi(0)$ is $\langle h^2\rangle/L_c^2$. In what follows we assume that $\chi(0) \ll 1$. Therefore we put

$$\boldsymbol{m} \to \begin{pmatrix}0\\0\\1\end{pmatrix}$$

in all pre-exponential factors excluding the arguments of δ-functions, where we use Taylor series expansions and keep linear terms in m_x and m_y. Now (10) reduces to

$$I^{spec}(t) = -\frac{\overline{h}}{(2\pi)^4}\frac{1}{z_0}\frac{1}{\chi(0)}\int \mathrm{d}\boldsymbol{m}\ \delta(m_z-1)\exp\left[-\frac{m_x^2+m_y^2}{2\chi(0)}\right]\sum_{qj\nu}\Theta(-q_z)q\frac{c_\nu^2}{c_j^2}n^0_{q\nu}(T_G)$$
$$\times r_{j\to\nu}[1-w(\omega_{q\nu})]\frac{1}{|\alpha_0|}\frac{z_0}{t+(1/c_\nu)(q/q_z)z_0}\,\delta\left(m_x-\frac{q_x}{q_z}\right)$$
$$\times\delta\left(2y_0+z_0\frac{\alpha_0 q}{q_z-\alpha_0 q}\frac{q_y}{q_z}-2y_0 f_0^{\nu j}m_y\right)$$
$$\times\delta\left(t+\frac{1}{c_\nu}\frac{q}{q_z}z_0-z_0\frac{c_\nu}{c_j^2}\frac{q}{q_z-\alpha_0 q}+t_0^{\nu j}m_y\right). \tag{11}$$

Here $\alpha_0\equiv\alpha(\boldsymbol{m}=\boldsymbol{i}_3)$ corresponds to the ideal surface, whilst

$$f_0^{\nu j}=-\frac{q_y^0 q_z^0}{(q_z^0-\alpha_0 q^0)^2}-\frac{q_z^0}{q_y^0}\qquad t_0^{\nu j}=-2y_0\frac{c_\nu}{c_j^2}\frac{q^0 q_z^0}{(q_z^0-\alpha_0 q^0)^2}$$

with q_y^0, q_z^0 and q^0 corresponding to the wave vectors for contributing phonons.

Despite its complexity (11) has simple meaning. The δ-functions in (11) give the selection of all possible paths with j-to-ν mode conversion at the surface (the first and second δ-functions) and determine the time taken to travel from generator to detector along the chosen trajectory (the third δ-function). The second δ-function sets the angles for incident and reflected phonons and after simple algebra may be written in the form

$$\frac{1}{z_0}\frac{1}{|A_0^{\nu j}(\vartheta_\nu^0)|}\delta[\vartheta_\nu-\vartheta_\nu^0+\xi_0^{\nu j}(\vartheta_\nu^0)m_y]$$

where $A_0^{\nu j}(\vartheta_\nu^0)$ and $\xi_0^{\nu j}(\vartheta_\nu^0)$ are dimensionless numerical factors of the order of 1 which are functions of the angle ϑ_ν^0, the reflection angle from the ideal surface (figure 2). The argument of the third δ-function can be rewritten in the form

$$t-\frac{z_0}{c_j\cos\vartheta_j}-\frac{z_0}{c_\nu\cos\vartheta_\nu}+t_0^{\nu j}m_y\qquad\text{or}\qquad t-\frac{z_0}{c_j\cos\vartheta_j^0}-\frac{z_0}{c_\nu\cos\vartheta_\nu^0}+\tau_0^{\nu j}m_y$$

where

$$\tau_0^{\nu j}=t_0^{\nu j}-\frac{z_0}{c_j}\frac{\sin\vartheta_j^0}{\cos^2\vartheta_j^0}(\vartheta_j-\vartheta_j^0)-\frac{z_0}{c_\nu}\frac{\sin\vartheta_\nu^0}{\cos^2\vartheta_\nu^0}(\vartheta-\vartheta_\nu^0).$$

The identification of the second term as the time t_j^0 taken by the phonon of the $\boldsymbol{k}j$-mode to travel from the generator to the part of the surface where it is reflected to the $\boldsymbol{q}\nu$-mode is straightforward. The third term is the time t_ν^0 taken by the $\boldsymbol{q}\nu$-phonon to travel from the point of its creation to the detector, while the last term accounts for the local normal variations. With these remarks formula (11) can be easily integrated. We give only the final result. In order to discuss the difference between the specular signals reflected from the ideal and smooth irregular surface we give both results:

$$I_{ideal}(t)=\sum_{\nu j}A_{\nu j}\,\delta(t-t_{\nu j}^0) \tag{12}$$

where $t_{\nu j}^0=t_\nu^0+t_j^0$ and $A_{\nu j}$ give the total detected intensity for the νj-pulse. Then

$$I^{spec}(t)=\sum_{\nu j}\varphi_j A_{\nu j}\frac{1}{\sqrt{2\pi\chi(0)}}\frac{1}{\tau_0^{\nu j}}\exp\left[-\left(\frac{t-t_{\nu j}^0}{\tau_0^{\nu j}}\right)^2\frac{1}{2\chi(0)}\right] \tag{13}$$

where

$$\varphi_j = \left(\int_0^\infty \mathrm{d}\omega\ \omega^3 n^0(\omega)[1 - w(\omega, j)]\right) \Big/ \left(\int_0^\infty \mathrm{d}\omega\ \omega^3 n^0(\omega)\right)$$

is the numerical factor accounting for the reduction in specular component due to diffuse scattering from short-scale irregularities. Inspection of (13) shows that the phonon pulse half-width is given by

$$\Gamma_{\nu j} = 2\sqrt{2\chi(0)}\tau_0^{\nu j} \approx \frac{\sqrt{\langle h^2\rangle}}{L_c} t_{\nu j}^0. \tag{14}$$

Thus it scales both with $\tau_0^{\nu j}$ which is equal to the time of flight of j-to-ν mode conversion as a result of reflection at the surface, and also with the pair correlation function of the surface roughness. It is also seen to be independent of the wavelength. This is not surprising, since we kept only zeroth-order approximation terms for $\bar{\lambda}/L_c \ll 1$ and in this limit pulse broadening is a purely geometrical effect, determined by reflection from a distribution of local mirrors.

5. Diffuse scattering

Now we discuss the diffuse component of the signal. Keeping only zeroth-order terms in long-range surface roughness in (8) and integrating over $\mathrm{d}\boldsymbol{x}'$, $\mathrm{d}t'$ we arrive at

$$I^{diff}(t) = -\frac{\bar{h}}{z_0^2} \sum_{\boldsymbol{k}j;\boldsymbol{q}\nu} \Theta(k_z)\Theta(-q_z) w(\boldsymbol{k}j \to \boldsymbol{q}\nu) c_\nu q q_z^2 n_{\boldsymbol{k}j}^0(T_G)\, \delta\left(q_x - q_z \frac{k_x}{k_z}\right)$$
$$\times \delta\left(q_y - q_z \frac{k_y}{k_z} + 2q_z \frac{y_0}{z_0}\right) \delta\left(t + \frac{z_0}{c_\nu}\frac{q}{q_z} - \frac{z_0}{c_j}\frac{k}{k_z}\right). \tag{15}$$

Integrating over $\mathrm{d}\boldsymbol{q}$ in (15) with the use of elastic nature of scattering from surface roughness and using the set of variables k, $\boldsymbol{\rho}$ and α rather than spherical coordinates when performing integration over $\mathrm{d}\boldsymbol{k}$ ($\boldsymbol{\rho}$ is the vector in the x–y-plane, so that $\boldsymbol{k} = -\boldsymbol{x}_G + \boldsymbol{\rho}$, and α is the angle between $\boldsymbol{\rho}$ and the y axis) we arrive at

$$I^{diff}(t) = z_0^2 \frac{V}{(2\pi)^3} \sum_{\boldsymbol{k}j} \int_0^\infty \mathrm{d}k\ k^2 \bar{h}\omega n_{\boldsymbol{k}j}^0(T_G)$$
$$\times \int_0^\infty \mathrm{d}\rho \int_0^{2\pi} \mathrm{d}\alpha\ \tilde{w}\left(k\frac{-\boldsymbol{x}_G + \boldsymbol{\rho}}{|-\boldsymbol{x}_G + \boldsymbol{\rho}|}, j \to \frac{c_j}{c_\nu} k \frac{\boldsymbol{x}_D - \boldsymbol{\rho}}{|\boldsymbol{x}_D - \boldsymbol{\rho}|}, \nu\right)$$
$$\times \frac{\rho}{[(z_0^2 + \rho^2 + y_0^2)^2 - 4\rho^2 y_0^2 \cos^2\alpha]^{3/2}}$$
$$\times \delta\left(t - \frac{1}{c_j}\sqrt{z_0^2 + \rho^2 + y_0^2 + 2\rho y_0 \cos\alpha}\right.$$
$$\left. - \frac{1}{c_\nu}\sqrt{z_0^2 + \rho^2 + y_0^2 - 2\rho y_0 \cos\alpha}\right). \tag{16}$$

Here we introduced the new function $\tilde{w}$ which is given by straightforward integration over $\mathrm{d}\boldsymbol{q}$. This expression for the diffusive signal may be easily analysed for a number of different cases.

First we discuss the signal shape at distant times exceeding the time of flight for the specular signal: $c_{j(\nu)}t \gg 2y_0$. Taking $\rho \to \infty$ in (16), we obtain

$$I^{diff}(t) = \frac{z_0^2}{(2\pi)^2} \sum_{\nu,j} \int_0^\infty \mathrm{d}k\ k^2 \bar{h}\omega n_{kj}^0(T_G) \tilde{w}_{j\nu}^{back}\left(\frac{z_0}{t}\left(\frac{1}{c_j} + \frac{1}{c_\nu}\right)\right) \frac{1}{t^5}\left(\frac{1}{c_j} + \frac{1}{c_\nu}\right)^4. \tag{17}$$

The expression (17) contains the probability for pure back-scattering of incident phonons with the conversion into different modes. Phonons in the tail of the diffusive signal arriving at the detector are scattered from spots on the surface separated from the origin by much more than the distance from the generator to the detector and, hence, returned along the same path. We keep the dependence of the back-scattering probability on the incident phonon wave vector and assume that it depends only upon the cosine of the incidence angle. Using Nakayama's approach [7, 8] we may calculate $\tilde{w}_{j\nu}^{back}$ for different pairs of modes.

This reproduces the shape of signal obtained by Nakayama for $c_{j(\nu)}t \to \infty$. However, for $y_0 \neq 0$ and $t \geq t_{j\nu}^0$ the shape of the signal will be very different. To illustrate this, we consider only the case where incident and scattered phonons possess the same velocity: $c_j = c_\nu = c$, i.e both are transverse. Now the general formula (16) can be significantly simplified. The argument of the δ-function in (16) then equals zero when

$$\rho_\pm = \pm\frac{ct}{2}\sqrt{\frac{c^2t^2 - 4(z_0^2 + y_0^2)}{c^2t^2 - 4y_0^2\cos^2\alpha}}. \tag{18}$$

Integration over $\mathrm{d}\rho$ is thus easily performed to give

$$I_{c_j=c_\nu=c}^{diff}(t) \propto \frac{1}{t}\int_0^{2\pi}\mathrm{d}\alpha\ \frac{1}{1 - 4y_0^2\cos^2\alpha/c^2t^2}\,\frac{1}{(\rho_+^2 + z_0^2 + y_0^2)^2 - 4\rho_+^2 y_0^2\cos^2\alpha}. \tag{19}$$

Substituting (18) into (19) and integrating over $\mathrm{d}\alpha$ we obtain finally

$$I_{c_j=c_\nu=c}^{diff}(t) \propto \frac{1}{t^5}\,\frac{t^4 + \frac{1}{2}\zeta^2 t_0^2(t^2 - t_0^2)}{t^4 - 2\zeta^2 t_0^2(t^2 - \frac{1}{2}t_0^2)}. \tag{20}$$

Here

$$t_0 = \frac{2\sqrt{(y_0^2 + z_0^2)}}{c}$$

is the time of flight and ζ is the geometrical factor

$$\frac{y_0}{\sqrt{z_0^2 + y_0^2}}.$$

To derive (20) we assumed that the rate of scattering from the surface is the same to all final states regardless of the direction of propagation. The use of Nakayama's differential cross-sections obviously changes this result [7, 8].

It is evident from (20) that the second factor which accounts for the finite spatial separation between the generator and detector significantly modifies the shape of the signal near the maximum, making the signal fall after the maximum much faster than for the geometry of back-scattering.

It is useful at this point to discuss the power dependences for diffuse and specular signals. If we neglect diffuse scattering, then the specular component scales with power dissipated in the generator P. At low generator temperatures, thus, $I_{spec}(t) \propto T_G^4$. Diffuse scattering causes the dependence on T_G to be slower (due to the factor φ_j in (13)). The diffuse signal (16) is obviously characterized by a faster rise with P or T_G. In the simplest case of low power levels (low temperatures) this immediately gives P^2 (or T_G^8), arising from T_G^4 due to lattice energy, and an additional T_G^4 to the scattering probability $\tilde{w} \propto \omega^4 \propto T_G^4$. This assumption is valid in the limit $\bar{\lambda}_{ph} \gg l_c$. As was mentioned above, the differential scattering cross-section $\tilde{w}_{j\to\nu}$ is related to $\sigma(J \to J')$ calculated by Nakayama, and therefore for each pair of modes we may take corresponding formulas from [7, 8]. We now discuss how the results are modified if we assume the irregular surface to be Gaussian with a finite correlation

length l_c. Calculation of the factor $\langle|\Delta\rho(\boldsymbol{k}'+\boldsymbol{q}')|^2\rangle$ [7, 8], defining the strength of coupling between incident and scattered modes yields

$$\langle|\Delta\rho(\boldsymbol{k}'+\boldsymbol{q}')|^2\rangle = \pi\rho_0^2 l_c^2\langle h^2\rangle \exp\left[-\frac{(\boldsymbol{k}'+\boldsymbol{q}')^2 l_c^2}{4}\right]. \tag{21}$$

Here $\Delta\rho(\boldsymbol{r})$ is a random part of the crystal density at the irregular surface, and $\boldsymbol{k}'$ and $\boldsymbol{q}'$ are 2D wave vectors—projections of 3D wave vectors for incident and scattered waves on the surface plane. All the results in [7, 8] were obtained for the case of white-noise irregularities, i.e. $\psi(\boldsymbol{r}) = \text{constant} \times \delta(r)$. For this case $\langle|\Delta\rho(\boldsymbol{k}'+\boldsymbol{q}')|^2\rangle = \text{constant}$. A finite length of correlation, thus, adds an exponential factor and modifies the pre-exponential constant, expressing it in terms of the correlation length and mean squared height of the surface irregularities. Therefore, we may keep Nakayama's differential cross-sections in the further analysis, simply multiplying them by the exponential factor in (21). Clearly, for long phonon wavelengths $\frac{1}{4}|\boldsymbol{k}'+\boldsymbol{q}'|l_c \ll 1$, so the exponential factor is not significant, and this is exactly the limit of applicability for Nakayama's theory. If, however, $\bar{\lambda}_{ph}$ becomes comparable to l_c, then the exponential factor in (21) plays the role of an effective cut-off, separating the spectral ranges of long and short wavelengths for phonons of the heat pulse.

We now go back to the expression (16), add the exponential factor, and again integrate over $\mathrm{d}\rho$ for the most important experimental case $c_j = c_v = c$. Again with ρ_+ from (18) we obtain

$$I^{diff}(t) = z_0^2\frac{V}{(2\pi)^3}\frac{1}{t}\int_0^\infty \mathrm{d}k\; k^2\hbar\omega n^0_{kj}(T_G)\int_0^{2\pi}\mathrm{d}\alpha\;\frac{\tilde{w}(k,\rho_+,\alpha)}{z_+z_-(1-(4y_0^2/c^2t^2)\cos^2\alpha)}$$
$$\times\exp\left[-\beta\left(1-\frac{z_0^2(\rho_+^2+y_0^2+z_0^2)}{z_+z_-}+\frac{y_0^2-\rho_+^2}{\sqrt{z_+z_-}}\right)\right] \tag{22}$$

where $z_\pm = \rho_+^2+z_0^2+y_0^2\pm 2\rho_+ y_0\cos\alpha$ and $\beta = \omega^2 l_c^2/4c^2$. First we note that in the geometry of back-scattering ($y_0 = 0$) the expression in square brackets in the exponent goes to zero. For $y_0 \neq 0$ it is always positive and varies slightly with α, the corresponding parameter being

$$\frac{1}{2}\frac{y_0^2}{y_0^2+z_0^2}\cos^2\alpha\left(\frac{t_0}{t}\right)^2.$$

We may analyse the temporal and temperature behaviour of the diffuse signal approximately by taking correction terms with $\cos\alpha$ equal to zero. Then

$$I^{diff}(t) \propto \frac{T^8}{t^5}\int_0^\infty \mathrm{d}z\,\frac{z^7}{\exp z-1}\exp(-\gamma^2 z^2) \tag{23}$$

where

$$\gamma = \frac{l_c}{c}\frac{k_B T_G}{\hbar}\frac{y_0}{\sqrt{2(y_0^2+z_0^2)}}\frac{t_0}{t} = \frac{T_G}{T^*}\frac{t_0}{t}.$$

Here

$$T^* \equiv \frac{c\hbar}{k_B l_c}\frac{2\sqrt{(y_0^2+z_0^2)}}{y_0}.$$

For $\gamma \ll 1$ we have $I^{diff}(t,T_G) \propto T_G^8 t^{-5}$. For $\gamma \gg 1$ we have $I^{diff}(t,T_G) \to T_G^8 t^{-5}\gamma^{-7} \propto T_G^1 t^2$. If $\gamma(t_0) \ll 1$, then $\gamma(t) \ll 1$ for $t \geq t_0$ and $I^{diff}(t)$ follows a $1/t^5$-law. However, if $\gamma(t_0) \gg 1$, then the signal first starts to rise, and then saturates at around

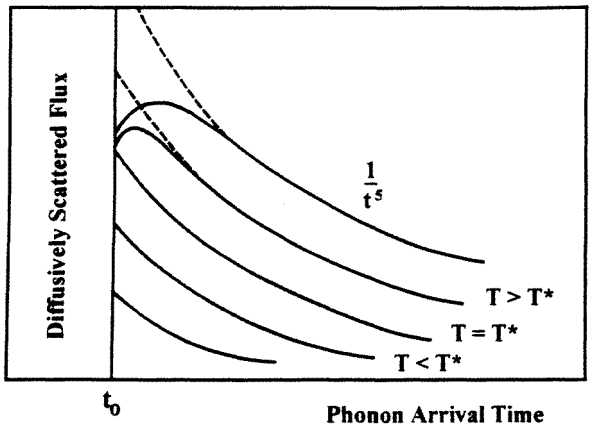

Figure 3. The behaviour of the diffusively scattered flux, I^{diff}, as a function of the arrival time for various values of the generator temperature, T_G.

$t_m = t_0 T_G/T^*$, reverses and asymptotically approaches $1/t^5$. Schematically this is illustrated in figure 3. As follows from the results of this analysis, if $T_G > T^*$ the signal peak shifts from the time-of-flight position and broadens. Note that if $T_G < T^*$ the peak half-width (or the related quantity $\tau_{60\%}$—the time taken for the signal to fall by 60% from its maximum value)—are independent of the power (temperature). When T_G approaches T^*, the signal half-width and $\tau_{60\%}$ (although to calculate $\tau_{60\%}$ one now has to take into account the power-dependent position of the signal peak) acquire power dependence. Both the half-width and $\tau_{60\%}$ are monotonically rising functions of power (temperature).

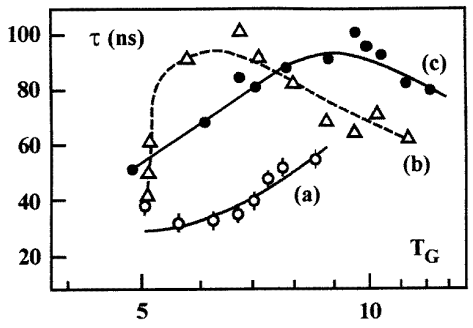

Figure 4. Experimental data for $\tau_{60\%}$ for samples (a) unimplanted, (b) implanted, and (c) implanted and annealed.

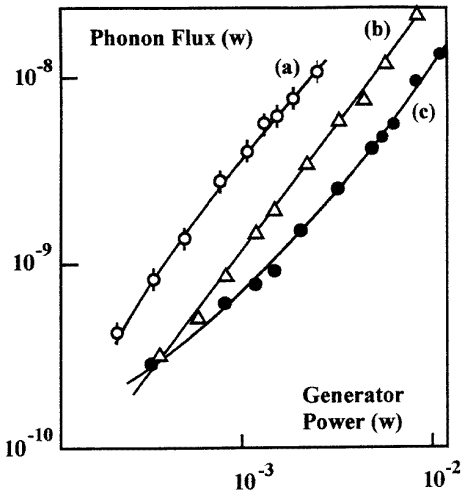

Figure 5. The observed magnitude of the TT peak as a function of generator power for the same conditions as in figure 4.

6. Discussion: comparison with experiment

We have obtained a general expression for the diffusive scattering peak as a function of arrival time, t, and heat pulse generator temperature, T_G. The result is expressed in terms of the dimensionless parameter, γ, itself a function of the ballistic time of flight of the specularly scattered phonons, and of the roughness scale of the surface. We were able to compare this model with the previous results of heat pulse experiments on an implanted silicon wafer in which the short-range correlation length, l_c, could be changed [9]. An amorphous layer was first produced below the surface of the wafer by ion bombardment. The interface between the amorphous and the crystalline regions is known to have two distinct roughness scales, one of long range produced by the statistical nature of the bombardment process, and one of short range relating to dislocations [11]. Careful annealing at an appropriate temperature can remove the dislocations without affecting the long-range irregularity. Figure 4 shows the variation as a function of the heat pulse generator temperature, T_G, of $\tau_{60\%}$, the time taken for the observed TA→TA scattering peak to fall by 60% of its maximum value under the conditions (a) before ion implantation with diffusive scattering taking place from the true surface of the crystal, (b) after implantation when both long-range order, L_c, and short-range order, l_c, were present, and (c) after annealing which increased l_c. Finally figure 5 shows the power dependence of the TA→TA peak for the same three conditions.

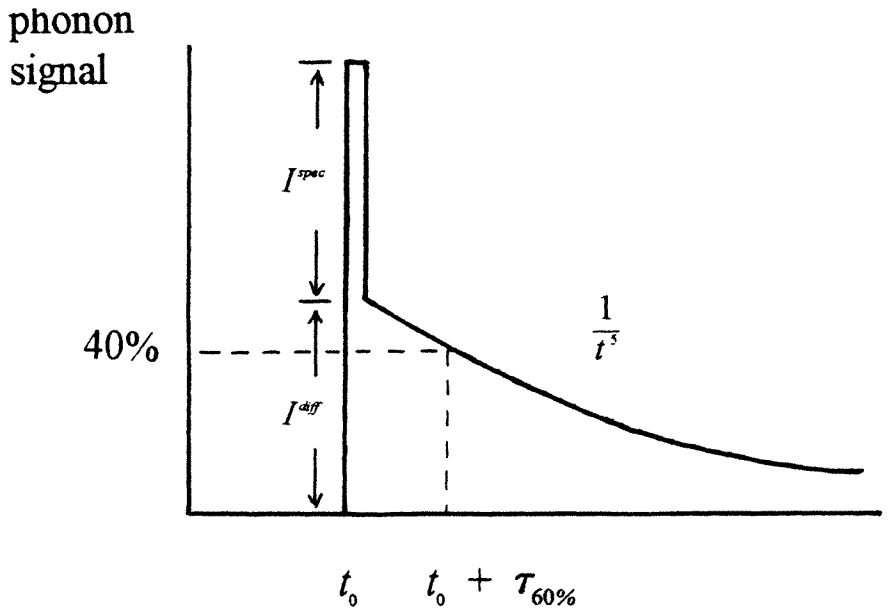

Figure 6. The detected phonon signal is the superposition of the specular, I^{spec}, and diffusive, I^{diff}, signals. The time $\tau_{60\%}$ is the measured time interval after the specular arrival time, t_0, which the signal falls by 60% of its peak value.

We consider first the pre-implanted data. We assume that the surface is polished to such a high grade that over the whole range of generator power the dominant phonon wavelength is still greater than l_c. We can describe the signal at the bolometer as the superposition of

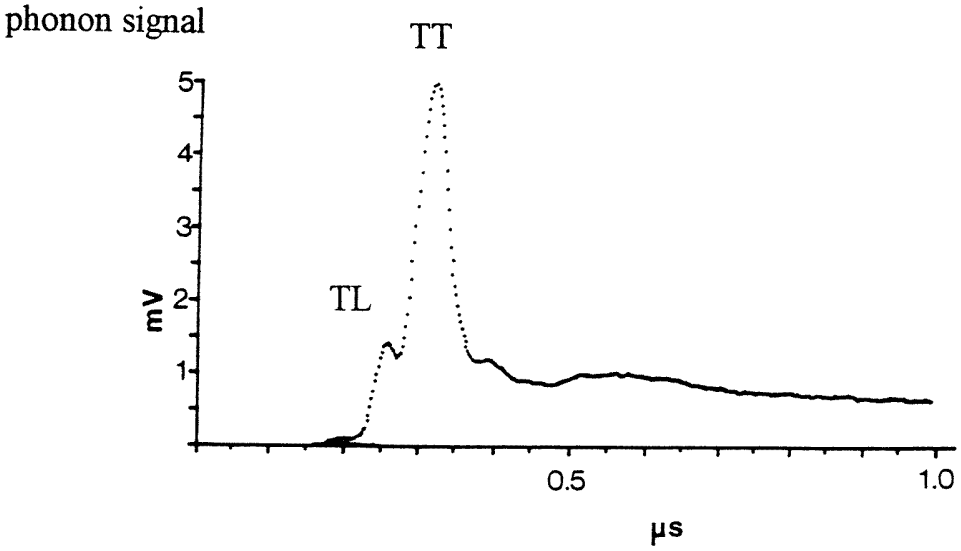

Figure 7. An experimental trace for comparison with the idealized model of figure 6. TT refers to transverse–transverse scattering, and TL to transverse–longitudinal scattering.

specular and diffusive peaks (figure 6), so the total signal may be written as

$$I(t) = I^{spec}(T_G) + I^{diff}(T_G)\left(\frac{t_0}{t}\right)^5 = I^{spec}(T_G)\left[1 + \zeta(T_G)\left(\frac{t_0}{t}\right)^5\right] \tag{24}$$

where $\zeta(T_G)$ is the ratio of diffuse to specular maxima and we also assumed the specular signal to be narrow and disregarded its temporal dependence arising from that. For comparison, the experimentally observed signal is shown in figure 7. TT refers to TA→TA scattering, and TL to the mode-converted signal. Any LL scattering is insignificantly small.

Using (24) we arrive at

$$\tau_{60\%} = t_0\left[1.20\left(\frac{\zeta(T_G)}{1+\zeta(T_G)}\right)^{0.2} - 1\right]. \tag{25}$$

Assuming $\bar{\lambda}_{ph} > l_c$ we must take $\zeta(T_G) \propto T_G^4$ or $\zeta(P) \propto P$. Thus $\zeta(P) = \zeta_0 P/P_0$ with ζ_0 to be estimated at the lowest power level from experimental data. For a polished sample prior to implantation (curve (a) in figure 5) this gave $\zeta_0 \cong 2.3$ that is, the diffuse signal at its maximum exceeds the specular signal at the lowest power of $P = 3 \times 10^{-4}$ W by a factor of 2.3. At the power level $P' = 3 \times 10^{-3}$ W we will have $\tau'_{60\%} \cong 50$ ns in close agreement with experimental data (figure 4, (a)). It is worth noting that the TT peak power dependence also finds a reasonable explanation if we take into account the fact that at low power levels $P \geq P_0$ we have $I^{diff}(P) \propto P^2$ and $I^{diff} \geq I^{spec}$. The experimental slope in the range $2 \times 10^{-4} \leq P \leq 8 \times 10^{-4}$ W is $\approx P^{1.7}$ with the exponent 1.7 being close to but less than 2 as it should be in the absence of diffusive scattering. The change of slope for higher P is an indication that the diffuse scattering cross-section does not follow a Rayleigh law at higher power levels, when a noticeable fraction of phonon energy is in the short-wavelength part of the spectrum approaching the lateral scale l_c of the polished surface.

After implantation the shape of the TT signal and its half-width change dramatically, reflecting the fact that now phonon scattering takes place not at the crystal surface, but at the irregular interface between damaged and crystalline regions. Both the shape of the observed signal and the TT amplitude variation with phonon generator power show only a small amount of specular reflection to be present at low power levels. This is obviously due to the diffuse scattering being much stronger than for the unimplanted sample. Presumably, for the implanted sample the spectrum of density irregularities in a damaged layer is broad, and so at a particular phonon power level there are many irregularities present with scales comparable to all phonon wavelengths. Then after implantation even at the lowest power level we are close to the top of the family of curves depicted in figure 3. On this basis we may interpret the experimental results of figure 5, (b) and (c). Firstly, we find experimental confirmation for our assumption from data in figure 5—see (b), showing the variation with the phonon generator power of the TT amplitude for the implanted sample. At low power levels the slope is given by $P^{0.75}$ in agreement with our initial assumption, since we expect the dependence to be slower than $\propto P$ if we stay close to T^*. The rise of the phonon generator power brings about a weakening of diffuse scattering which should eventually saturate with power. The specular component which is still power dependent then emerges above the diffuse signal, thus providing a gradual change of slope towards the dependence $\propto P$, as indeed is seen in figure 5—see (b). The dependence of $\tau_{60\%}$ on P is also consistent with our assumption. Firstly, $\tau_{60\%}$ rises with power in agreement with our analysis when the diffuse signal dominates. However, this behaviour reverses when the specular component 'overtakes' the diffuse component, and more phonons form the specular signal which is characterized by a half-width due to the angular spread of local normals in the eikonal regime. If we anneal the sample, then we remove most of the short-range irregularities leaving, however, longer-scale irregularities. Therefore, the $\tau_{60\%}$ versus P curve saturates and reverses at lower phonon generator powers. Almost throughout the measured range of phonon generator powers the slope of the signal versus phonon generator power is slightly higher than 1 (approximately 1.2–1.3), except for at the very beginning (low power levels) for sample (c) where there appears a slight indication for a slope below unity, which would be consistent with $\tau_{60\%}$ increasing with P. Finally, we note that the exponent 1.2–1.3 seen for the annealed sample (curve (c)) and the implanted sample without annealing (curve (b)) can be understood as a contribution arising from the power variation of the numerical factor φ_j in (13), which above T^* obviously decreases, while diffuse scattering weakens, thus making the overall dependence slightly faster than $P^{1.0}$.

Thus we find that the data observed for this novel series of experiments are in general agreement with our analytical expressions for both specular and diffuse scattering from rough surfaces with both long- and short-range irregular components. For Gaussian irregular surfaces with a finite correlation length for short-scale irregularities l_c we have shown that signal half-widths turn out to be wavelength dependent and experimental data confirm this. In contrast the dependences of the half-widths for the two signals were independent of phonon wavelength in the white-noise model for short-range irregularities. In this model, however, an observable half-width variation with phonon generator power may be found due to interplay between different power dependencies of specular and diffusive signal amplitudes. We expect then a gradual change of half-width from one power-independent value to another, corresponding to either broadening or narrowing of the peak.

In summary, we have considered the scattering of heat pulses from rough surfaces and interfaces modelled in terms of two extreme length cases. We derived, for the first time, analytic expressions which described both diffusive and specular components of a scattered heat pulse consisting of phonons of all wavelengths, not just those in long- or short-

wavelength limits. Our expressions describe satisfactorily the main experimental features of heat pulse scattering in which the length scale can be varied.

Acknowledgments

Support from the EPSRC, MONBUSHO and the British Council is gratefully acknowledged.

References

[1] bin Rani H, Edwards S C, Wigmore J K and Collins R A 1989 *Surf. Interface Anal.* **14** 850
[2] Taborek P and Goodstein D L 1980 *Phys. Rev.* B **22** 1550
[3] Mok E, Burger S, Dottinger S, Lassmann K and Eisenmenger W 1986 *Phys. Lett.* **114A** 473
[4] bin Rani H, Edwards S C, Wigmore J K and Collins R A 1988 *J. Phys. C: Solid State Phys.* **21** L701
[5] Muller G and Weis O 1990 *Z. Phys.* B **80** 25
[6] Kozorezov A G 1983 *Phys. Lett.* **98A** 261
[7] Nakayama T 1985 *Phys. Rev.* B **32** 777
[8] Nakayama T 1986 *Phys. Rev.* B **33** 8664
[9] Strickland K R, Edwards S C, Wigmore J K, Collins R A and Jeynes C 1992 *Surf. Interface Anal.* **18** 631
[10] Kozorezov A G, Wigmore J K, Miyasato T and Strickland K 1995 *Proc. Phonons'95 (Sapporo)* ed T Nakayama
[11] Roorda S, Doorn S, Sinke W C, Scholte P M L O and van Loene E 1989 *Phys. Rev. Lett.* **62** 1880